Vol. 23, No. 1(2024) Poly24218
Revista Mexicana de Ingeniería Química

Effect of chitosan on the electrokinetic, spectroscopic, and textural properties of TiO_2 nanoparticles

Efecto del quitosano en las propiedades electrocinéticas, espectroscópicas y texturales de nanopartículas de TiO_2

K. Macías-Collado[1], L.T. Ballesteros-Rozo[2], V. W. Velázquez-Vázquez[1], D.M. Frías-Márquez[3], R. López-González[3], M.A. Alvarez-Lemus[1]*

[1]*Laboratory of Bioassays and Environmental Testing, Academic Division of Engineering and Architecture, Juarez Autonomous University of Tabasco, Tabasco, México*

[2]*University of America, Bogota, Colombia.*

[3]*Nanotechnology Laboratory, Academic Division of Engineering and Architecture, Juarez Autonomous University of Tabasco, Tabasco, México.*

Received: November 29, 2023; Accepted: January 19, 2024

Abstract

Titania (TiO_2) nanoparticles were synthesized using the sol-gel method and subsequently modified with chitosan (CS). FTIR spectroscopy confirmed the presence of chitosan by modifications on the 3380 cm^{-1} and 1630 cm^{-1} bands, while XRD showed a shift in the reflection peaks from titania when it was bound to chitosan. TGA revealed that the actual amount of chitosan added to the composite was about 16% wt. Hydrodynamic diameter for titania particles was 720 nm, whereas the composite exhibited mainly particles of 1098 nm. Zeta potential measurements showed a change from -13.7 to 21 mV for TiO_2-CS compared to pure titania. Physisorption analysis determined the BET specific surface area of TiO_2 and TiO_2-CS being 38 m^2/g and 24 m^2/g, respectively. In the visual observation, the behavior of titania and TiO_2-CS suspended in deionized water for 24 hours was observed. Contact angle measurements were taken over calcite artificial rocks using brine, brine/TiO_2, and brine/TiO_2-CS, resulting in angles of 113.73°, 106.8°, and 97.90°, respectively. Although they fall within the hydrophobic range, a decrease in contact angle was achieved by adding nanoparticles. Sedimentation and agglomeration of titanium particles were formed at shorter time than for the composite suspended particles.

Keywords: Chitosan, TiO_2, nanoparticles, particle stability, contact angle.

Resumen

Las nanopartículas de titania (TiO_2) se sintetizaron mediante el método sol-gel y posteriormente se modificaron con quitosano (CS). La espectroscopia FTIR confirmó la presencia de quitosano mediante modificaciones en las bandas de 3380 cm^{-1} y 1630 cm^{-1}, mientras que la DRX mostró un cambio en los picos de reflexión de la titania cuando se unió al quitosano. TGA reveló que la cantidad real de quitosano añadida al compuesto era de aproximadamente el 16% en peso. El diámetro hidrodinámico de las partículas de titania fue de 720 nm, mientras que el compósito exhibió principalmente partículas de 1098 nm. Las mediciones del potencial zeta mostraron un cambio de -13,7 a 21 mV para TiO_2-CS en comparación con titania pura. El análisis de fisisorción determinó que el área superficial específica de TiO_2 y TiO_2-CS es de 38 m^2/g y 24 m^2/g, respectivamente. En la observación visual se observó el comportamiento de titania y TiO_2-CS suspendidos en agua desionizada durante 24 horas. Las mediciones del ángulo de contacto se realizaron sobre rocas artificiales de calcita utilizando salmuera, salmuera/TiO_2 y salmuera/TiO_2-CS, lo que dio como resultado ángulos de 113,73°, 106,8° y 97,90°, respectivamente. Aunque se encuentran dentro del rango hidrofóbico, se logró una disminución en el ángulo de contacto mediante la adición de nanopartículas. Se observó sedimentación y aglomeración de partículas de titanio, mientras que para el compuesto se observaron partículas suspendidas durante un período más largo.

Palabras clave: Quitosano, Nanopartículas, TiO_2, estabilidad de partículas, ángulo de contacto.

*Corresponding author. *E-mail*: mayra.alvarez@ujat.mx;
https://doi.org/10.24275/rmiq/Poly24218
ISSN:1665-2738, *issn-e*: 2395-8472

1 Introduction

The research in nanoparticles (NP) has exponentially increased during the last years, because of the interest of improving the properties of bulk materials. In this sense, metal oxide nanoparticles are attractive because are relatively easy to obtain and their characteristics can be tuned by slightly modifying their synthesis parameters. Among these type of nanoparticles, titanium dioxide (TiO_2) is one of the most explored metal oxides due to its multiple applications such as catalyst, photocatalyst, sensor, drug carrier, among others. Given its low toxicity, chemical stability, low price, and the versatility of the methods for obtaining TiO_2 has attracted attention also for its fabrication at nanoscale. Among the different methods for obtaining TiO_2 nanoparticles, the sol-gel is a simple procedure in which the use of different precursors significantly affects the features of the final product. In oil and gas industry, TiO_2 nanomaterials have attracted attention due to their potential for decontamination of water (Ángel-Hernández *et al*., 2021; Ramírez-Revilla *et al*., 2023), and recently as additives in recovery fluids to improve the current enhanced oil recovery methods either by modification of surface tension or interfacial interactions (Khalilnezhad *et al*., 2019; González-Calderón *et al*., 2021; Negi *et al*., 2021) However, as many other metal oxides the most limiting feature is related to its low stability in aqueous media since agglomeration takes place when no additives are added (Qi *et al*., 2013; Kao & Cheng, 2020). For overcoming this disadvantage, TiO_2 has been modified with different compounds such as surfactants (Li *et al*., 2017) and some polymers like PEG, or chitosan (CS) (Gozdecka & Wiacek, 2017; Karthikeyan *et al*., 2017), a polysaccharide derived from chitin that has generated great interest due to its low cost and non-toxicity (Rodríguez-Guzmán *et al*., 2022). Nevertheless, most of the work reported on literature on nano-TiO_2 with chitosan it has been directed to biomedical applications such as drug delivery, due to the pH-sensitivity of chitosan, or even as antibacterial composites and biosensing (Ozerin *et al*., 2006; Siripatrawan & Kaewklin, 2018; Anaya-Esparza *et al*., 2020; Dos Santos *et al*., 2023). Because of chitosan is easy to obtain, and due to its high biocompatibility, biodegradability and very low environmental impact, chitosan has found applications also in oil and gas industry, mainly due to the adsorption capacity of the composites for the removal of pollutants from water, and when used in combination with other nanomaterials such as graphene, removal of heavy metals and ions can be achieved (Fahimehsadat *et al*., 2019). In Enhanced Oil Recovery (EOR), nanoparticles of metal oxides such as SiO_2 and ZnO have been investigated as components of fluids used in flooding such as brine or CO_2, where amounts of nanoparticles lower than 0.1%w/v, have demonstrated potential in the recovery of oil due to their specific surface area and the surface chemical composition of the nanoparticles which promotes interactions between the fluid and the rock with oil (Tajmiri *et al*., 2015; Negi *et al*., 2021). On the other hand, it has been reported that chitosan and its derivatives, showed an important effect on altering properties such as rock wettability, viscosity and oil-water interfacial tension which makes this compound, suitable for flooding in EOR applications (Chen *et al*., 2020; Dos Santos *et al*., 2020; 2023), but because the biological behavior of chitosan it is also related to its molecular weight and degree of deacetylation, improvement of physicochemical properties of TiO_2 cannot be taken for granted, and specific studies should be performed in order to assess synergistic effect. Despite the proved potential of both materials separately, investigation on the use of CS-TiO_2 nanocomposites for EOR are scarce, even though synergistic effect between these two materials on wettability has been reported (Ładniak *et al*., 2021). In this work, the synthesis of CS-TiO_2 nanocomposite was performed to evaluate the effect of the polymer on the electrokinetic properties of titanium oxide, and thus to improve its colloidal stability in saline solution for further application as additive in nanofluids for flooding in EOR. To analyze the effect of chitosan in the improvement of the properties of TiO_2, the materials were characterized through techniques such as Fourier transformed infrared spectroscopy (FTIR), X-ray diffraction (XRD), scanning transmission electron microscopy (STEM), thermogravimetric analysis (TGA), Z potential, dynamic light scattering (DLS), surface area and pore size distribution (N_2 physisorption) and contact angle.

2 Materials and methods

2.1 *Synthesis of the TiO_2 Nanoparticles*

The titanium dioxide nanoparticles (TiO_2 NP) were synthetized by the sol-gel method as previously reported by Poluboyarinov (2019). Briefly, 16 mL of sodium hydroxide (NaOH, Meyer, 0.015 M) were added to 15 mL of ethanol (C_2H_6O, Meyer, 99.5%). The mixture was cooled down to -5°C, during 2 h. Then 22 mL of Titanium (IV) isopropoxide (TTIP, $C_{12}H_{28}O_4Ti$, Aldrich, 97%) were added dropwise under constant stirring (1200 rpm) at room temperature, after the addition of the alkoxide the solution was kept under stirring for 24 h. The sample was rinsed thrice with 20 mL of deionized water and placed in a drying oven (Ecoshel, 9023A) at 60 °C for 12 h. Afterwards, the solid sample was calcined

at 500°C for 4 h at a heating rate of 1°C/min (Terlab, TE-M12D).

2.2 Modification of TiO_2 with low-molecular weight chitosan

For obtaining the titanium dioxide particles with chitosan (TiO_2-CS), a two-steps procedure was followed. First, a 2.5% w/v solution of low-molecular weight chitosan (Sigma Aldrich, 75-85% deacetylated) in 100 mL of acetic acid solution (1% v/v) was prepared and kept under stirring (1200 rpm for 24 h) until CS was fully dissolved. The solution was reserved for further use. In a vessel, 0.5 g of TiO_2 NP were suspended into 50 mL of deionized water and sonicated for 20 min, then 50 mL of the CS solution were added to obtain a composite with a 2.5:1 ratio (CS:TiO_2), the suspension was stirred at 1200 rpm for 4 h. Finally, the TiO_2-CS particles were separated by centrifugation (Civeq, 80-2) at 4000 rpm for 15 min. The solid particles were dried at 60 °C for 12 h (Ecoshel, 9023A). The obtained TiO_2-CS particles were stored for characterization.

2.3 Characterization of the nanomaterials

The crystalline phases for TiO_2 and TiO_2-CS powders were characterized by X-ray diffraction using an X-Ray Diffractometer (DRX) (Bruker Advance Eco) D8 Advance Eco, with a source of Cu (K_α =1.5406 Å) from 10° to 70° (2θ),0.020 step, and t=0.4 s. The presence of different functional groups were identified through Fourier Transform Infrared spectroscopy (FTIR), in the 4000 to 400 cm^{-1} range using a Nicolet iS50 FTIR spectrometer (Thermo Fisher Scientific). For this, 1%wt. of each sample was mixed with potassium bromide (KBr, Meyer, 98%), and pressed (3 ton, PIKE hydraulic press) using a stainless steel pelletizer to obtain thin 10 mm in diameter pellets, which were analyzed in the transmission accessory of the equipment. Transmission Electron Microscope (JEOL, JEM-2100) operating at 200 V was used for determining the size and shape of the particles, samples were suspended in isopropyl alcohol, sonicated during 5 min, and then placed in a 300-mesh copper grid (Ted Pella Inc.). For the zeta potential (ζ) and hydrodynamic size measurements, 1%wt. of each sample was suspended in 10 mL of water and the measurements were carried out in a Zetasizer Nano Zs (Malvern Panalytical) with DTS1070 and DTS0012 disposable cells, respectively. Thermal properties were characterized by Thermogravimetric Analysis (TGA) in a Labsys evo 1100 (Setaram) equipment from 100-600 °C, at 10°K/min rate under Ar atmosphere (20 psi). Specific surface area, pore size distribution and fractal dimension coefficients were obtained from N_2 isotherms measured in an Autosorb iQ (Quantachrome instruments), prior to adsorption the samples were outgassed at 100°C for 13 h.

2.4 Visual stability of nanoparticles suspensions

The stability in water of the TiO_2 and TiO_2-CS nanoparticles was visually evaluated as follows: different suspensions were prepared by adding 0.01 g of either TiO_2 or TiO_2-CS in 10 mL of deionized water. Then each suspension was sonicated for 20 min and left 24 h in a stable place avoiding vibrations. The sedimentation of the particles as function of time was recorded using a conventional camera at different times.

2.5 Contact angle measurements

The contact angle was measured to determine whether the addition of NP to water, modifies the interactions between the surface of artificial calcite rocks and the nanofluid. To obtain the contact angle, calcium carbonate tablets ($CaCO_3$, Sigma Aldrich, 99.9%) were prepared as follows: 3.2 g of calcium carbonate were dried it at 100 °C for 12 h. Then, the $CaCO_3$ was pressed (4 ton) in a pelletizer to obtain small cylindrical pellets, which were further thermally treated at 100°C for 12 h, to remove moisture. The pellets were soaked into a baker with a sample of crude oil (Well SP-904, Tabasco México) previously heated to 60 °C for 24 h. Finally, the calcite+oil pellets were dried at 50 °C for 24 h. The contact angle was measured for brine alone 3% w/v NaCl (Meyer, 98%), and the following nanofluids: brine+TiO_2 and brine+TiO_2-CS, the nanofluids were prepared by suspending 100 mg of each NP in 100 mL of 3% w/v NaCl. For this, the oil-soaked pellets were placed on the holder of a home-made device equipped with automatized injection system, and then a drop of each fluid was injected on the surface of the pellet. The images were taken and then processed using ImageJ software for measuring the angles between the surface of the oil-soaked pellets and the nanofluids.

3 Results and discussion

3.1 Powder XRD

Figure 1 shows the XRD patterns for TiO_2 and TiO_2-CS nanomaterials. As it is widely known, anatase, brookite and rutile are the TiO_2 polymorphs commonly formed at atmospheric pressure, and depending on the synthesis method preferential growth of crystals takes place to obtain any of these crystalline structures which turns out in different properties

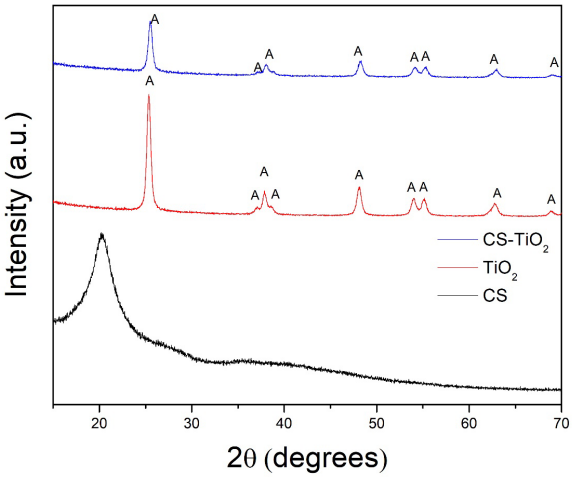

Fig 1. XRD patterns of the as-synthesized samples and chitosan, A indicates the anatase planes.

associated to a specific structure (Zhang *et al*., 2017; Hiroi, 2022).

Anatase and rutile phases are the most chemically stable structures for TiO_2, and those with the larger number of applications (Xiaoping, 2022). According to Figure 1, the XRD pattern for TiO_2 exhibited several peaks located at 25.33°, 37.87°, 48.122°, 53.98°, 55.15°, 62.79° and 68.86° (2θ) which correspond to the reflections (101), (004), (200), (105), (211), (204) and (116) respectively, these peaks agree with the PDF card 00-021-1272 for anatase phase. From the XRD pattern of the TiO_2-CS sample, the presence of CS cannot be confirmed due to the absence of the characteristic broad peak at 20.28°(2θ), this could be attributed to the loss of crystallinity of chitosan after the interaction with TiO_2 nanoparticles, leading to an amorphous configuration undetected by XRD. This structural change has already been reported when chitosan interacts with other substances at a nanoscale (Ali *et al*., 2018). Nevertheless, slight shifts in the position of the peaks toward higher angles, were observed. Additionally, the intensity of the peaks for TiO_2-CS sample, was lower compared to the TiO_2 XRD pattern. This can be attributed to potential interactions between TiO_2-CS, as reported by others (Al-Taweel *et al*., 2019; Hussein *et al*., 2021) where it has been described that the decrease in the signal may be attributed to a strong interaction through hydrogen bonds between titanium dioxide and chitosan, which may take place by incorporating TiO_2 particles between chitosan chains resulting in no modification of crystallite size (Table 1). The average crystallite size, D was estimated using the Scherrer equation (Eq. 1), as described by Hussein, *et al.* (2021).

$$d = \frac{K\lambda}{\beta \cos\theta} \tag{1}$$

Where λ represents the X-ray wavelength (Cu (K_α =1.5406 Å)), β is the corrected value (radians) of the Full Width at Half Maximum (FWHM) obtained in degrees from the diffractogram. The K value used was 0.9, which is suitable for spherical particles (Hassanzadeh-Tabrizi, 2023).

Table 1. Properties of the as-synthesized materials.

Sample	S_{BET} (m^2/g)	C (BET)	Mean pore size (nm)	Crystallite size (nm)	ζ (mV)
TiO_2	38.1	42.8	7.86	18.10	-26.0
TiO_2-CS	24.0	68.8	7.78	19.54	+17

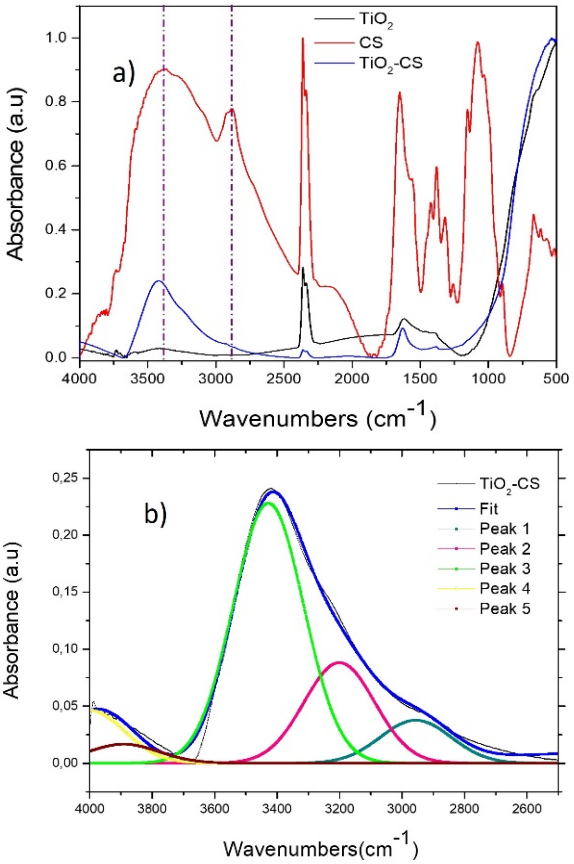

Fig 2. a) FTIR full spectra of the samples, b) TiO_2-CS Gaussian fitting of the 4000-2600 cm^{-1} infrared zone.

3.2 *FTIR spectroscopy*

The analysis by infrared spectroscopy provides valuable information on the presence of functional groups. Since the middle infrared region was studied, the expected information is about the organic moiety due to the polymer. In Figure 2a, the corresponding spectra for TiO_2, TiO_2-CS and CS are displayed. As the samples were pressed into KBr, small bands between 1500 and 1250 cm^{-1} were observed even in the TiO_2 samples, which are attributed to KBr impurities (Goriletsky *et al*., 2001). The FTIR spectrum for pure chitosan shows a characteristic peak at 3380 cm^{-1} which is assigned to the stretching vibrations of -OH groups from glucosamine, the peak

centered at 2883 cm^{-1} corresponds to the stretching of -C-H bonds, around 1653 cm^{-1}, 1383 cm^{-1} and 1077 cm^{-1} which are associated with the vibration bands for C=O, C-H and O-H, and C-O, respectively and are related to the amide (Siripatrawan & Kaeklin, 2018; Hussein *et al*., 2021).

On the other hand, the TiO_2 spectra shows a band located at 512 cm^{-1} attributed to the vibrations of Ti-O-Ti groups, while the peak present in 1617 cm^{-1} is due to the hydroxyl groups probably from adsorbed water molecules, these two bands are similar to those observed for the TiO_2-CS sample. The characteristic bands for chitosan around 1650 and 2880 cm^{-1} are not observed in the spectrum for TiO_2-CS, due to the broad bands around 1630 and the one between 2800 and 3600 cm^{-1}. By looking closer the 4000-2600 cm^{-1} region of the TiO_2-CS spectrum, differences in the intensity and location compared to bare TiO_2 can be observed. This band can be attributed to the presence of water molecules adsorbed from the environment and due to the presence of surface hydroxyl groups from the oxide. For the TiO_2 sample, this band is centered ca. 3415 cm^{-1} whereas for the TiO_2-CS sample is shifted to 3423 cm^{-1}. From the observation of CS spectrum, it can be assumed that this shift may be interpreted because of the interactions between the surface hydroxyl groups from titania and the hydroxyl and amine groups from chitosan (Branca *et al*., 2016). By resolving the peak between 4000-2500 cm^{-1} for the TiO_2-CS spectrum (Figure 2b), it can be clearly observed the asymmetry of the band, interpreting this as the contribution of more than one signal. A low-intense band around 2900 cm^{-1} is now clear. Two additional bands from the resolved signal can be attributed to vibrations of the -OH groups but from two different species, one from the hydroxylated surface of the TiO_2 (~3350 cm^{-1}) and another from the glucosamine moiety of chitosan (~3380 cm^{-1}). With this analysis, it can be assumed the presence of chitosan in the TiO_2-CS sample, and the shifts observed in the band at high wavenumbers can be assumed as the result of the interactions between both materials (Anaya-Esparza *et al*., 2020).

3.3 N_2 physisorption

Nitrogen adsorption isotherms of bare TiO_2 and TiO_2-CS samples are displayed in Figure 3. TiO_2 is generally a mesoporous material when obtained by sol-gel process, with relatively large specific area. From the adsorption-desorption isotherm we can observe that it resembles a type IVa isotherm (Thommes *et al*., 2015), which is commonly exhibited by mesoporous materials with the characteristic presence of hysteresis loop. In this case, the plateau at relative pressures above 0.8 is absent indicating two possibilities: the incomplete filling of mesopores or the presence of macropores, although it can be

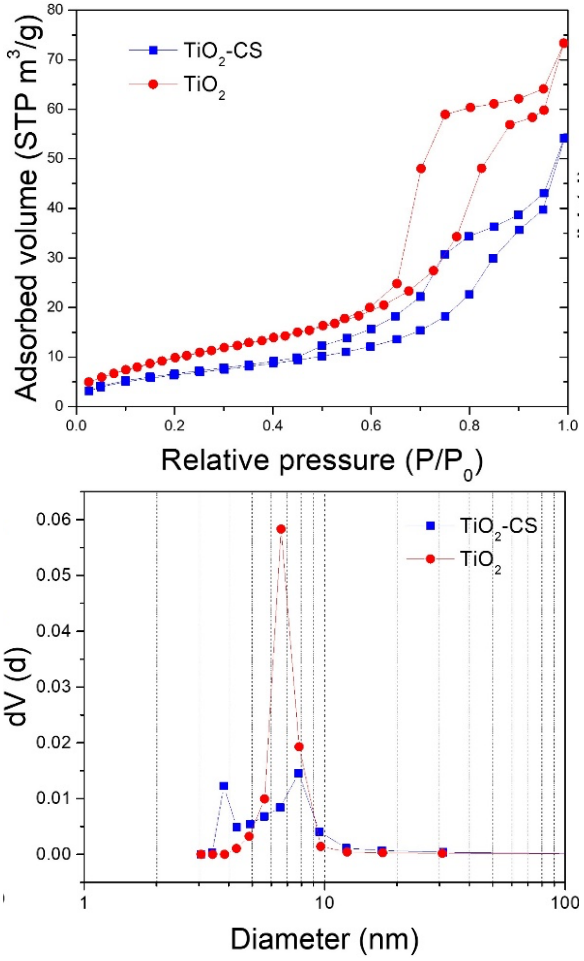

Fig 3. a) N_2 adsorption isotherms at 77K of the TiO_2-based NP, and b) Pore size distribution obtained by BJH model from desorption data.

observed that between 0.78 and 0.95 a small step is formed. The isotherms for both samples (TiO_2 alone and TiO_2-CS) are similar in shape, but with different adsorbed volume amounts, being TiO_2-CS the sample that adsorbed the lower amount of gas. Regarding the specific BET area (S_{BET}) of the samples, the values estimated from adsorption data between relative pressure ranges of 0.5-0.3, when chitosan is added to TiO_2, a 36% decrease in S_{BET} value compared to the specific area of TiO_2. Similar observations have been made by others, when CS is used to form TiO_2-CS nanocomposites where a significant decrease in S_{BET} has been reported, depending on the content of the biopolymer when prepared by crosslinking procedure (Al-Taweel *et al*., 2019). It is worth to mention that the method did not promote the obtaining of materials with high-specific area. In this sense, it has been reported that when using titanium isopropoxide, specific areas can vary from 16 m^2/g up to values close to 150 m^2/g, depending on the calcination temperature and morphology of the obtained particles, being particularly low when fibers or rods are obtained (Surovčík *et al*., 2022;

Padmini *et al*., 2021). In the case of the TiO_2-CS material, the decrease in surface area can be attributed to the occlusion of TiO_2 pores, since the method for incorporating the CS along with the amount of the polymer added, will promote surface covering affecting the porosity of the TiO_2, limiting the access of N_2 to the pores. The calculated BET constant C for each material provides an idea on the interactions between the adsorbent and the adsorbate; for the TiO_2 sample C=42.8 which indicates low interactions and thus low heat of adsorption, while for the TiO_2-CS this value increased to 68.8, which may indicate the presence of chitosan on the surface of TiO_2, that is now responsible for the interactions with the N_2 molecules and somehow favors the interactions. It can be hypothesized that despite the presence of chitosan the adsorbent-adsorbate interactions in monolayer are stronger than for bare TiO_2, the specific surface area decreased probably due to the fact of a lower number of pores, which is somehow confirmed by the pore size distribution plot (PSD, Figure 3b). Nevertheless, since BET theory is an approximation, further experiments will be needed to understand how the chitosan affects the adsorption heat of the TiO_2 surface.

Regarding the PSD, it can be seen that TiO_2 sample exhibited a narrower distribution than TiO_2-CS and threefold the adsorbed volume. The mean pore size was close to each other (Table 1), but with slight difference in the distribution, since for TiO_2 PSD showed monomodal and narrower distribution while the distribution for TiO_2-CS exhibited two sizes (3.8 and 7.7 nm), this could be explained assuming that when chitosan is combined with TiO_2, probably the biopolymer particles or the film formed on TiO_2 leave some small voids among them which can be interpreted as smaller pores.

3.4 *Thermogravimetric analysis*

It is important to estimate the experimental amount of chitosan incorporated by the simple procedure here carried out. With this idea in mind, thermogravimetric analysis was performed to both samples: the TiO_2 calcined and the TiO_2-CS. In Figure 4, a comparison among bare titania, the composite and pure chitosan is shown. In order to dismiss the presence of physically adsorbed water from the ambient, the samples were first heated up to 100°C, then the treatment from 100-600°C was performed. For the TiO_2 sample, the total amount of loss mass was nearly zero, which was expected since the sample was already thermally treated at 500°C. From the thermogram of the sample TiO_2-CS, a 4% weight loss between 100-250°C was observed, followed by a second one loss of nearly 12%, these can be attributed to the presence of chitosan since its primary degradation starts around 247°C and it is completed below 450°C (Kumar & Koh, 2012). This can be confirmed by the thermal

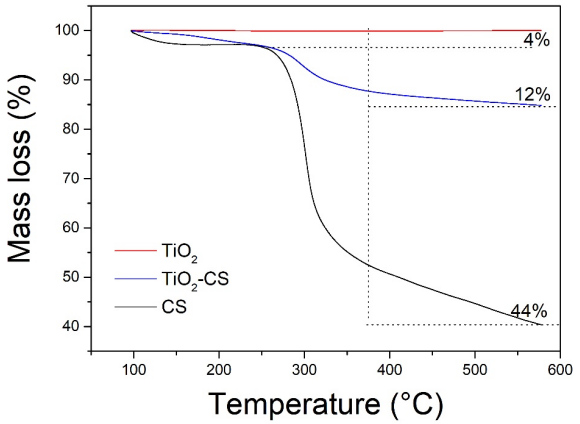

Fig 4. TGA of the samples TiO_2, TiO_2-CS and CS previously dried at 100°C.

behavior exhibited by pure chitosan. Based on these results, it can be assumed that thermal stability of chitosan was not affected by TiO_2, and that the total amount of chitosan added on the TiO_2 particles was about 16%. According to the preparation method, the nominal chitosan:TiO_2 ratio used was 2.5:1, then we can assume from the TGA that only 16% of chitosan was adsorbed on the surface of the titanium oxide, it can be noticed the low amount of chitosan that remains in the sample, however it is important to notice that incorporation of the polymer was tried to be achieved without addition of any linker molecule. Impregnation is a feasible method for incorporating a variety of compounds on the surface of TiO_2 nanomaterials, nevertheless the efficiency is related to the nature of the molecule which in this case seemed to have moderate affinity for the polymer.

3.5 *STEM analysis*

The use of titanium isopropoxide usually promotes the obtaining of small particles with good dispersion. As expected, the sample of bare TiO_2 was formed by agglomerates of nanoparticles, the size of the small nanoparticles was lower than 50 nm approximately (Figure 5a), whereas for the sample with chitosan it can be observed that particles remain agglomerated, but a thin transparent film can be noticed over which nanoparticles seem to be immobilized, and the agglomerates look tightly packed (Figure 5b). When used in low concentrations Chitosan usually tends to coat nanoparticles, which has been used mainly for drug delivery applications and for metal oxide nanoparticles chitosan is commonly incorporated without the addition of any anchoring agent. Nevertheless, the efficiency of coating depends on several factors such as type of nanoparticle, molecular weight of the polymer, contact time and temperature (Frank *et al*., 2020). As shown by the TGA, the incorporation of chitosan was below the theoretical amount, probably due to the short time

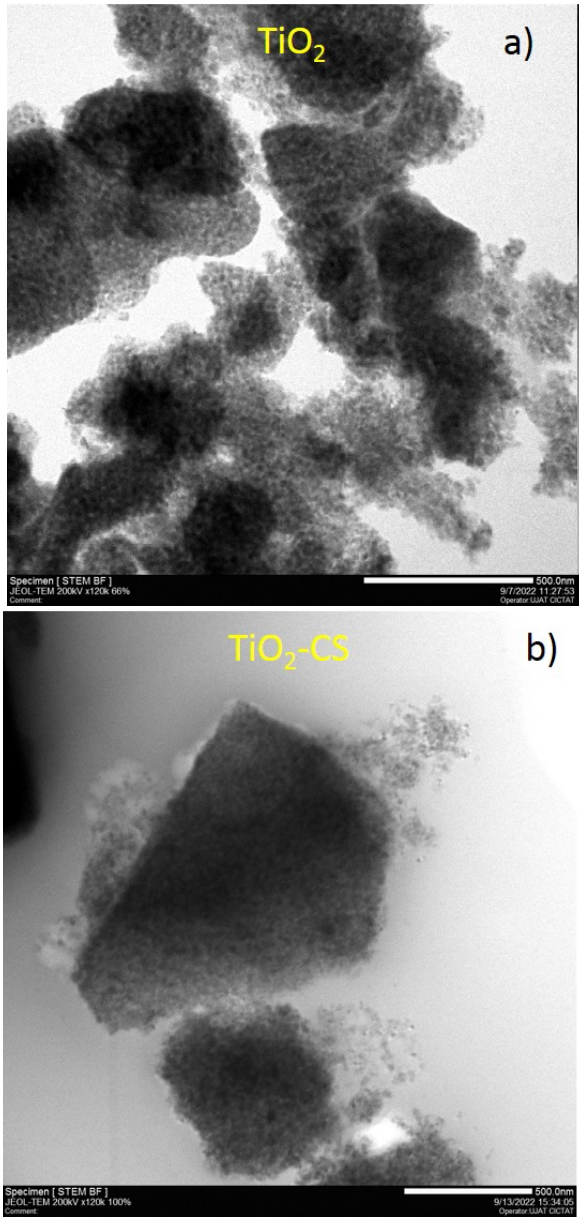

Fig 5. STEM images of the a) bare TiO_2 particles and b) chitosan-modified samples.

of contact. It should be also considered that because of the high chitosan:TiO_2 ratio (2.5:1) and the size of the titania particles, formation of chitosan-coated nanoparticles is not expected. It is widely accepted that behavior of nanoparticles can be altered by varying the amount of additives or modifiers, in this work we observed that despite the large CS:TiO_2 ratio used the actual amount of CS present in the sample was 16%w, thus it may be worth of further investigation to determine the effect of CS at lower concentration for obtaining coated nanoparticles, which could change the stability of the nanofluid through modifications in zeta potential, shape and agglomeration of TiO_2 nanoparticles.

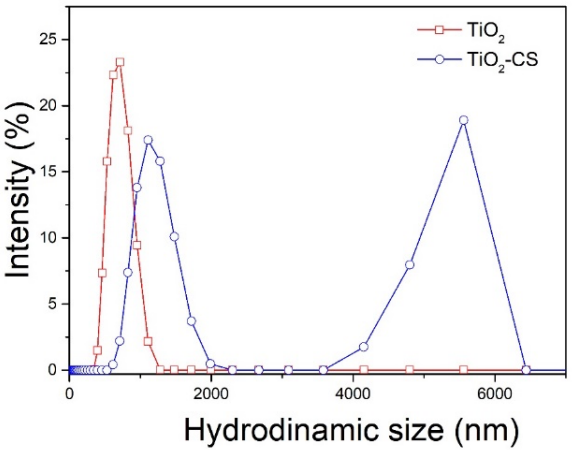

Fig 6. Hydrodynamic size obtained by DLS using water as dispersant.

3.6 Dynamic light scattering and Electrophoretic light scattering

It is widely known that hydrodynamic size is in general, larger than the size measured by microscopy. In the as-synthesized samples the exhibited different particle size distributions and the corresponding plots are shown in Figure 6. For bare TiO_2, the distribution shows one intense peak around 712 nm and a relatively narrow distribution, compared to that observed for the nanocomposite, which exhibits a bimodal distribution with larger sizes. These results can be due to the agglomeration of the particles that increases when suspended in water. The extremely large sizes may obey to the presence of large particle-agglomerates attached to chitosan, as can be inferred from the microscopic analysis.

STEM images confirmed the size and distribution of the bimodal particles of TiO_2-CS, most of the particles are forming large agglomerated, however there are smaller particles that could be attributed to titanium with a lower aggregation of chitosan.

The zeta potential for TiO_2 was electronegative (-13.7 mV) but when chitosan was incorporated this parameter changed to +21 mV. The change in the zeta potential can be attributed to the electrostatic force between positive charges of CS and negative charges of TiO_2. Even though CS load is about 16% according to TGA analysis, the zeta potential of the nanocomposite was significantly shifted, mainly due to the contribution of the positive zeta potential of the polymer (Lin *et al.*, 2015), similar behaviors have been also observed for different types of nanoparticles when coated with chitosan (Frank *et al.*, 2020). The zeta potential values provide a criterion for nanoparticle suspension stability, although major stability is reached at values larger than ±30 mV, it has been reported that chitosan improves stability even at low zeta potential values (Schubert & Chanana, 2019).

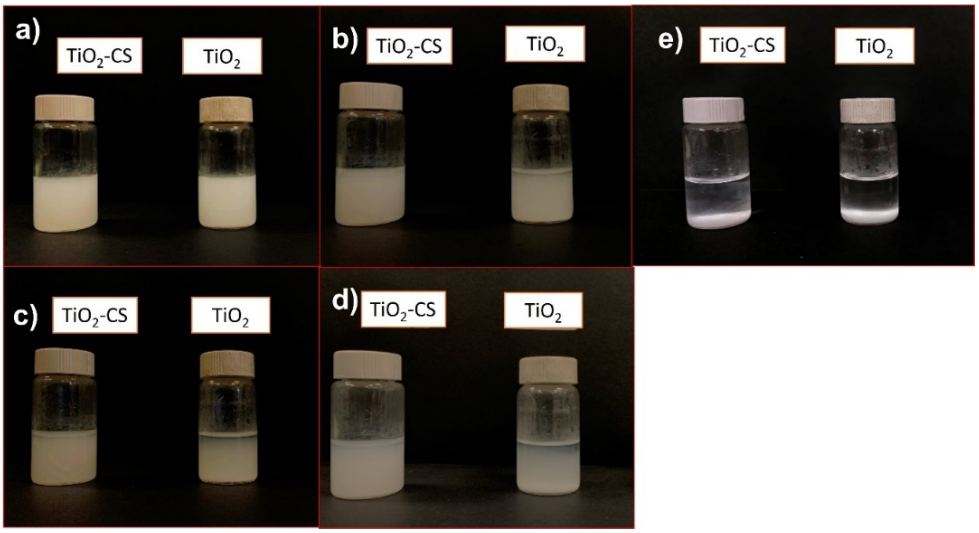

Fig 7. Visual stability test of TiO_2-CS compared to TiO_2 in deionized water at different times a) 0 min, b) 30 min, c) 60 min, d) 90 min, e) 24 h.

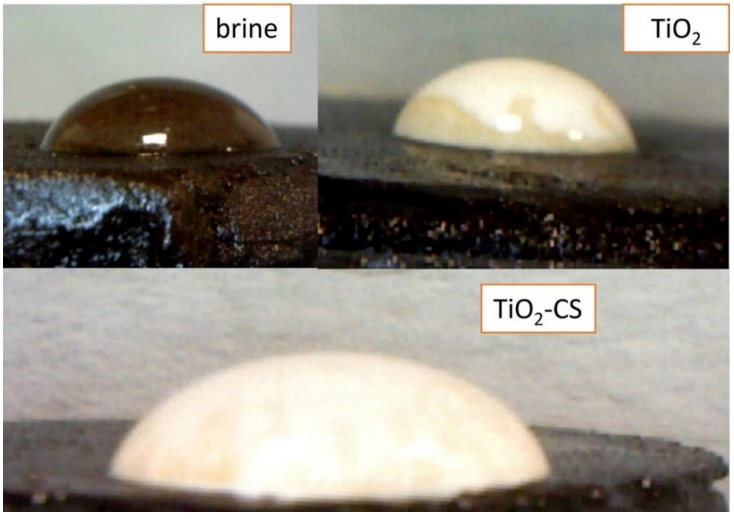

Fig 8. Contact angle for brine, brine+TiO_2 and brine+TiO_2-CS fluids over oil-soaked synthetic calcite rocks.

3.7 Visual test for particles suspension stability

For exploring the potential of these nanoparticles as nanofluids for Enhanced Oil recovery, the stability test was performed by visual inspection of the sedimentation of the nanoparticles. The nanofluids were left to precipitate for 24 h, and pictures were taken at different times (Figure 7). One of the main disadvantages for industrial applications of nanoparticles is their tendency to precipitation when no additives are added. For avoiding this, usually cationic surfactants are incorporated in nanofluids but due to its synthetic nature, concerns about their toxicity limits the application of NP. In recent years, the use of organic and biodegradable surfactants or surface modifiers has been explored such as cellulose and PEG (Shi *et al*., 2021; Zhu *et al*., 2021), to promote greener approaches. In this scenario chitosan shows potential as coating agent increasing the stability of nanoparticles and modifying interfacial tension (Zheng & Lian, 2015; Dos Santos *et al*., 2023), but TiO_2-CS composites have not been explored so far. For this, determining of the stability of the nanofluid is a desired property. As it can be observed, at t=0 both fluids were cloudy indicating that the nanoparticles are suspended, after 30 min a thin clear layer at the top of the TiO_2 nanofluid appears, indicating that sedimentation process begins, but TiO_2-CS nanofluid remains stable. After 90 min, this upper translucent layer is more significant for the TiO_2 sample. After 24 h, the fluid with bare titania appears completely clear on the top while the nanoparticles can be observed in the bottom of the vial, whereas for the TiO_2-CS slightly cloudy solution is still observed.

According to the Derjagin-Landau-Verwey-Overbeek (DLVO) theory, it is mentioned that the

colloidal stability in the suspensions can be reduced by the zeta-potential of the samples. The smaller the zeta potential the bigger aggregation in the particles and greater sedimentation (Jonassen *et al*, 2012) however, for this experiment, the electropositive charge introduced by the chitosan improves the stability of TiO_2.

3.8 Contact angle measurements

For determining whether chitosan improves the surface interactions between oil and brine, a drop of each one prepared nanofluid was placed over the surface of the oil-soaked synthetic calcite pellets and the corresponding photographs are displayed in Figure 8. For the pure saline solution (Figure 8), the contact angle measured was $\theta = 113.7°$, whereas 106.8° and 97.9° were estimated for TiO_2 and TiO_2-CS nanofluids, respectively. From these values we observed that bare TiO_2 produces a slight change in the wettability of the oil-embedded calcite which has also been reported by other groups for different rocks (Bayat *et al*., 2014; Ehtesabi *et al*., 2015).

More significant was the reduction with the TiO_2-CS nanofluid, which according to the contact angle, the surface is now more water-wet. Usually, calcite rocks have affinity for oil molecules due to charge attraction, since oil organic molecules are negatively charge whereas calcite surface is positive, this makes carbonate rocks oil-wet surfaces. Based on the results, the nanofluids altered the interactions between brine and the calcite allowing the penetration of the saline fluid which may indicate an indirect modification on interfacial tension, since the original oil-wet surface shifted to a slightly water-wet surface and resulting beneficial for increasing the recovery of oil (Sun *et al*., 2018; Al-Ameer, 2023). It has been reported that TiO_2 nanoparticles combined with surfactants decreases the contact angle of carbonate asphalt rocks up to 42° at the same concentration (0.1%) after 30 days of aging and the suggested mechanism was through the adsorption of nanoparticles on the surface of the rock which further are adsorbed and penetrates the pores (Hou & Sun, 2021). However, more detailed test must be performed in order to fully understand how the nanocomposites interact with the oily surface of calcite.

Conclusions

Impregnation of titanium dioxide with chitosan allowed the obtaining of a hybrid nanocomposite with lower sedimentation rate than TiO_2 alone, but higher contact times could be explored to improve the efficiency of chitosan adsorption. The chemical properties of chitosan and its composition promotes changes on the surface of TiO_2 probably due to electrostatic forces due to anchoring of chitosan, provoking that the number of surface hydroxyl groups of TiO_2 are less available because organic groups of chitosan can be attached as the shifts on infrared signals suggest. The presence of chitosan modifies the porosity, size and zeta potential of the hybrid resulting composite. Despite the low value of zeta potential, TiO_2-CS showed more stability in water suspension than bare TiO_2, and it can be also related with the differences in contact angles which in both cases are lower than the one measured for brine alone. We assume that combination of zeta potential, modifications in surface composition which modifies the porosity of the nanocomposite facilitate the interactions of the brine and oil.

Acknowledgment

To DAIA-UJAT and LANNBIO-CINVESTAV Mérida for the facilities and the equipment acquired through CONACYT funding. We would also want to acknowledge the technical assistance given by S. Hernández for STEM measurements.

References

Al-Ameer, M.A., Sahib Azad, M., Al-Sheri, D., Mohamud, M., Shahzad Kamal, M., Patil, S. (2023). A guide for selection of aging time and temperature for wettability alteration in various rock oil. *ACS Omega 8*, 30790-30801. https://doi.org/10.1021/acsomega.3c00023

Ali, M.E.A., Aboelfadl, M.M.S., Selim, A.M., Khalil, H.F., & Elkady, G.M. (2018). Chitosan nanoparticles extracted from shrimp shells, application for removal of Fe(II) and Mn(II) from aqueous phases. *Separation Science and Technology 53*(18), 2870-2881. https://doi.org/10.1080/01496395.2018.1489845

Al-Taweel, S.S., Saud, H.R., Kadhum, A.A.H., Takriff, M.S. (2019). The influence of titanium dioxide nanofiller ratio on morphology and surface properties of TiO_2/chitosan nanocomposite. *Results in Physics 13*, 102296. https://doi.org/10.1016/j.rinp.2019.102296

Anaya-Esparza, L.M., Ruvalcaba-Gómez, J.M., Maytorena-Verdugo, C.I., González-Silva, N., Romero-Toledo, R., Aguilera-Aguirre, S., Pérez-Larios, A., Montalvo-González, A.E. (2020). Chitosan-TiO_2: A Versatile Hybrid Composite. *Materials (Basel) 13*, 811. https://doi.org/10.3390/ma13040811

Ángel-Hernández, B., Hernández-Aldana, F., Pérez-Osorio, G., Gutiérrez-Arias, J.E.M. (2021). Municipal wastewater treatment by photocatalysis: Comparison between UV lamp and solar radiation using TiO_2 and ZnO/TiO_2 synthesized catalysts. *Revista Mexicana de Ingeniería Química 20*(3), Cat2438. https://doi.org/10.24275/rmiq/Cat2438

Bayat, A.E., Junin, R., Samsuri, A., Piroozian, A., Hokmabadi, M. (2014). Impact of metal oxide nanoparticles on enhanced oil recovery from limestone media at several temperatures. *Energy Fuels 28*, 6255-6266. https://doi.org/10.1021/ef5013616

Branca, C., D'Angelo, G., Crupi, C., Khouzami, K., Rifici, S., Ruello, G., Wanderlingh, U. (2016). Role of the OH and NH vibrational groups in polysaccharide-nanocomposite interactions: A FTIR-ATR study on chitosan and chitosan/clay films. *Polymer 99*, 614-622. https://doi.org/10.1016/j.polymer.2016.07.086

Chen, Q., Ye, Z., Tang, L., Wu, T., Jiang, Q., Lai, N. (2020). Synthesis and Solution Properties of a novel hyperbranched polymer based on chitosan for enhanced oil recovery. *Polymers 12*, 2130. https://doi.org/10.3390/polym12092130

Dos Santos Francisco, A.D., Grasseschi, D. (2020). Wettability alteration of oil-wet carbonate rocks by chitosan derivatives for application in enhanced oil recovery. *Journal of Applied Polymer Science 138*, 50098. https://doi.org/10.1002/app.50098

Dos Santos Francisco, A.D., Maia, K.C.B., Vieira Moura, J.G., Veiga Nascimento, R.S., da Silva Lima, F., Grasseschi, D. (2023). Chitosan derivatives as surfactant carriers for enhanced oil recovery - Experimental and molecular dynamic evaluations of polymer-surfactant interactions. *Colloids and Surfaces A Physicochemical Engineering Aspects 671*, 131644. https://doi.org/10.1016/j.colsurfa.2023.131644

Ehtesabi, H., Ahadian, M., Taghikhani, V. (2015). Enhanced oil recovery using TiO_2 nanoparticles: Investigation of deposition during transport in core plug. *Energy Fuels 29*, 1-8. https://doi.org/10.1021/ef5015605

Fahimehsadat, V., Hossein, D. (2019). The characterization of TiO_2-reduced graphene oxide nanocomposites and their performance in electrochemical determination for removing heavy metals ions of cadmium (II), lead (II) and copper (II). *Materials Science and Engineering: B 243*, 189-198. https://doi.org/10.1016/j.mseb.2019.04.009

Frank, L.A., Onzi, G.R., Morawski, A.S., Pohlmann, A.R., Guterres, S.S., Contri, R.V. (2020). Chitosan as a coating material for nanoparticles intended for biomedical applications. *Reactive and Functional Polymers 147*, 104459. https://doi.org/10.1016/j.reactfunctpolym.2019.104459

González-Calderón, J.A., Peña-Juárez, M.G., Zarraga, R., Contreras-López, D., Vallejo-Montesinos, J. (2021). The role of alkoxysilanes functional groups for surface modification of TiO_2 nanoparticles on non-isothermal crystallization of isotactic polypropylene composites. *Revista Mexicana de Ingeniería Química 20*(1), 435-452. https://doi.org/10.24275/rmiq/Poly1995

Goriletzky V.I., Mitichkin A.I., Belenko L.E., Rebrova T.P. (2001) IR spectroscopy of KBr and salt and crystals. *Semiconductor Physics, Quantum Electronics & Optoelectronics 4*, 139-141. https://doi.org/10.15407/spqeo4.02.139

Gozdecka, A., Wiacek, A.E. (2017). Behavior of TiO_2/Chitosan dispersion as a function of solution pH. *Progress on Chemistry and Application of Chitin and its Derivatives 12*, 21-47. https://doi.org/10.15259/PCACD.22.03

Hassanzadeh-Tabrizi, S.A. (2023). Precise calculation of crystallite size of nanomaterials. *Journal of Alloys and Compounds 968*, 171914. https://doi.org/10.1016/j.jallcom.2023.171914

Hiroi, Z. (2022). Inorganic structural chemistry of titanium dioxide polymorphs. *Inorganic Chemistry 61*, 8393-8401. https://doi.org/10.1021/acs.inorgchem.2c00945

Hou, J., Sun, L. (2021). Synergistic effect of nanofluids and surfactants on heavy oil recovery and oil-wet calcite wettability. *Nanomaterials 11*(7), 1849. https://doi.org/10.3390/nano11071849

Hussein, E.M., Desoky, W.M., Hannafy, M.F., Guirguis, O.W. (2021). Effect of TiO_2 nanoparticles on the structural configurations and thermal, mechanical and optical properties of chitosan/TiO_2 nanoparticle composites. *Journal of Physics and Chemistry of Solids 152*, 109983. https://doi.org/10.1016/j.jpcs.2021.109983

Jonassen, H., Kjøniksen, A.L., Hiorth, M. (2012). Stability of chitosan nanoparticles cross-linked with tripolyphosphate. *Biomacromolecules 13*, 3747-3756. https://doi.org/10.1021/bm301207a

Kao, J.Y., Cheng, W.T. (2020). Study on dispersion of TiO_2 nanopowder in aqueous solution via near supercritical fluids. *ACS Omega 5*, 1832-1839 https://doi.org/10.1021/acsomega.9b03101

Karthikeyan, K.T., Nithya, A., Jothivenkatachalam, K. (2017). Photocatalytic and antimicrobial activities of chitosan-TiO_2 nanocomposite. *International Journal of Biological Macromolecules 104*, 1762-1773. http://dx.doi.org/doi:10.1016/j.ijbiomac.2017.03.121

Khalilnezhad, A., Rezvani, H., Ganji, P., Kazemzadeh, Y. (2019). A complete experimental study of oil/water interfacial properties in the presence of TiO_2 nanoparticles and different ions. *Oil & Gas Science and Technology 74*, 39. https://doi.org/10.2516/ogst/2019007

Kumar, S., Koh, J. (2012). Physiochemical, optical and biological activity of chitosan-chromone derivative for biomedical applications. *International Journal of Molecular Sciences 13*, 6102-6116. https://doi.org/10.3390/ijms13056102

Ładniak, A., Jurak, M., Wiącek, A.E. (2021). Physicochemical characteristics of chitosan-TiO_2 biomaterial. 2. Wettability and biocompatibility. *Colloids and Surfaces A: Physicochemical and Engineering Aspects 630*, 127546. https://doi.org/10.1016/j.colsurfa.2021.127546

Li, X., Yoneda, M., Shimada, Y., Matsui, Y. (2017). Effect of surfactants on the aggregation and stability of TiO_2 nanomaterial in environmental aqueous matrices. *Science of the Total Environment 574*, 176-182. https://doi.org/10.1016/j.scitotenv.2016.09.065

Lin, B., Luo, Y., Teng, Z., Zhang, B., Zhou, B., Wang, Q. (2015). Development of silver/titanium dioxide/chitosan adipate nanocomposite as an antibacterial coating for fruit storage. *LWT-Food Science and Technology 63*(2), 1206-1213. https://doi.org/10.1016/j.lwt.2015.04.049

Negi, G.S., Anirbid, S., Sivakumar, P. (2021). Applications of silica and titanium dioxide nanoparticles in enhanced oil recovery: Promises and challenges. *Petroleum Research 6*, 224-246. https://doi.org/10.1016/j.ptlrs.2021.03.001

Ozerin, A.N., Zelenetskii, A.N., Akopova, T.A., Pavlova-Verevkina, O.B., Ozerina, L.A., Surin, N.M., Kechek'yan, A.S. (2006). Nanocomposites based on modified chitosan and titanium oxide. *Polymer Science Series A 48*, 638-643. https://doi.org/10.1134/S0965545X06060137

Padmini, M., Balaganapathi, T., Thilakan, P. (2021). Mesoporous rutile TiO_2: Synthesis, characterization and photocatalytic performance studies. *Materials Research Bulletin 144*, 111480. https://doi.org/10.1016/j.materresbull.2021.111480

Poluboyarinov, A.S., Chelpanov, V.I., Lebedev, V.A., Kozlov, D.A., Khazova, K.M., Volkov, D.S., Kolesnik, I.V., Garshev, A.V. (2019). Titanium oxide microspheres with tunable size and phase composition. *Materials 12*(9), 1472. https://doi.org/10.3390/ma12091472

Qi, J., Ye, Y.Y., Wu, J.J., Wang, H.T., Li, F.T. (2013). Dispersion and stability of titanium dioxide nanoparticles in aqueous suspension: effects of ultrasonication and concentration. *Water Science and Technology 67*(1), 147-151. https://doi.org/10.2166/wst.2012.545

Ramírez-Revilla, S. A., Camacho-Valencia, D., & Ortiz-Romero, D. (2023). Kinetic evaluation of photocatalytic decoloration of Synozol Red K3BS dye using TiO_2-anatase and direct solar radiation. *Revista Mexicana de Ingeniería Química 22*(1), 2-7. https://doi.org/10.24275/rmiq/IA2995

Rodríguez-Guzmán, C. A., Montaño-Leyva, B., Sánchez-Burgos, J. A., Bautista-Rosales, P. U., & Gutierrez-Martinez, P. (2022). Chitosan and GRAS substances application in the control of Geotrichum candidum isolated from tomato fruits (*Lycopersicum esculentum* L.) in the state of Nayarit, Mexico: *In vitro* tests. *Revista Mexicana de Ingeniería Química 21*(3), Bio2790. https://doi.org/10.24275/rmiq/Bio2790

Schubert, J., Chanana, M. (2019). Coating matters: Review on colloidal stability of nanoparticles with biocompatible coatings in biological media, living cells and organisms. *Current Medicinal Chemistry 25*, 4556-4586. https://doi.org/10.2174/0929867325666180601101859

Shi, L., Zhang, J., Zhao, M., Tang, S., Cheng, X., Zhang, W., Li, W., Liu, W., Peng, H., Wang, Q. (2021). Effects of polyethylene glycol on the surface of nanoparticles for targeted drug delivery. *Nanoscale 13*, 10748-10764. https://doi.org/10.1039/D1NR02065J

Siripatrawan, U., Kaewklin, P. (2018). Fabrication and characterization of chitosan-titanium dioxide nanocomposite film as ethylene scavenging and antimicrobial active food packaging. *Food Hydrocolloids 84*,125-134. https://doi.org/10.1016/j.foodhyd.2018.04.049

Sun, X., Zhang, Y., Chen, G., Liu, T., Ren, D., Ma, J., Sheng, Y., Karwani, S. (2018). Wettability of hybrid nanofluid-treated sandstone/heavy oil/brine systems: implications for enhanced heavy oil recovery potential. *Energy and Fuels 32*, 11118-11135. https://doi.org/10.1021/acs.energyfuels.8b01730

Surovčík, J., Medvecká, V., Greguš, J., Gregor, M., Roch, T., Annušová, A., Ďurina, P., Vojteková, T. (2022). Characterization of TiO_2 nanofibers with enhanced photocatalytic properties prepared by plasma assisted calcination. *Ceramics International 48*, 37322-37332. https://doi.org/10.1016/j.ceramint.2022.08.309

Tajmiri M., Mousavi S.M., Reza Ehsani M., Roayaei E., Emadi A. (2015). Wettability alteration of sandstone and carbonate rocks by using ZnO nanoparticles in heavy oil reservoirs. *Iranian Journal of Oil & Gas Science and Technology 4*, 50-66. https://doi.org/10.22050/ijogst.2016.12479

Thommes, M., Kaneko, K., Neimark. A.V., Olivier, J.P., Rodriguez-Reinoso, F., Rouquerol, J., Sing, K.S. (2015). Physisorption of gases, with special reference to the evaluation of surface area and pore size distribution (IUPAC Technical Report). *Pure and Applied Chemistry 87*, 1051-1069. https://doi.org/10.1515/pac-2014-1117

Xiaoping, W. (2022). Applications of titanium dioxide materials. In *Titanium Dioxide - Advances and Applications*. Muhammad Ali H. (Ed) IntechOpen. https://doi.org/10.5772/intechopen.99255

Zhang, M., Tiedan, C., Wang, Y. (2017). Insights into TiO_2 polymorphs: highly selective synthesis, phase transition, and their polymorph-dependent properties. *RSC Advances 7*, 52755-52761. https://doi.org/10.1039/C7RA11515F

Zheng, X.F., Lian, Q. (2015). Synthesis and evaluation of CoFe2O4-chitosan nanoparticles in enhanced oil recovery. *Journal of Dispersion Science and Technology 36*, 245-251. https://doi.org/10.1080/01932691.2014.904794

Zhu, J., Xie, S., Yang, Z., Li, X., Chen, J., Zhang, X., Zheng, N. (2021). A review of recent advances and prospects on nanocellulose properties and its applications in oil and gas production. *Journal of Natural Gas Science and Engineering 96*, 104253. https://doi.org/10.1016/j.jngse.2021.104253